

Stellar populations in brightest cluster galaxies

S. Iani Loubser^{1,2}, Patricia Sánchez-Blázquez^{2,3}, Ilona Soechting⁴, Anne Sansom²



¹ University of the Western Cape, Cape Town, South Africa;
² Jeremiah Horrocks Institute, University of Central Lancashire, Preston, UK;
³ Instituto de Astrofísica de Canarias, Tenerife, Spain;
⁴ Astrophysics, University of Oxford, Oxford, UK.



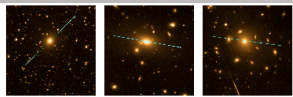
Introduction

Brightest cluster galaxies (BCGs) have been modelled dynamically and imaged extensively. However, their formation mechanism is still unknown. Mergers between smaller galaxies, massive star formation in the early stages of the formation of the cluster due to (the now extinguished) cooling flows, or monolithic collapse that may originate from unusually large primordial fluctuations, are all possible candidates. These processes will leave different imprints in the dynamical properties and in the detailed chemical abundances of the stars.

The current study of the stellar populations in brightest cluster galaxies (BCGs) aims to set constraints on the formation and evolution of these objects. We have presented the largest optical, spatially-resolved, spectroscopic sample of BCGs to date (Loubser et al. 2008, 2009). The sample contains high signal-to-noise ratio, long-slit observations for 49 BCGs in the nearby Universe, taken with the Gemini North and South and WHT telescopes. This sample allows possible connections between the kinematical, dynamical and stellar population properties to be studied using a statistically significant number of galaxies. The spatially-resolved kinematic profiles for 49 BCGs were measured, and SSP-equivalent ages, metallicities and α -abundance ratios in the centres of 43 BCGs were derived using the Lick/IDS system of absorption line indices. The indices measured and parameters derived for the BCGs were compared with those of ordinary ellipticals in the same mass range. They were also tested for possible correlations with the kinematic properties of the galaxies (velocity dispersion, rotation) and the properties of the host clusters (density, mass, distance to X-ray peak, presence of cooling flows).

Galaxy Sample, Observations and Data Reduction

We selected and observed a statistically significant sample of nearby BCGs over a 20 month period (2006 - 2008). The selection methods and criteria are described in Loubser et al. (2008). A subset of 10 of the brightest galaxies selected were observed at the 4.2m WHT telescope in June 2006. Further to this, we obtained 41 galaxies with the GEMINI North and South telescopes in the 2006B, 2007A and 2007B observing semesters. The data reduction procedures are described in the above-mentioned paper. Line strength indices depend on the broadening of lines caused by the velocity dispersion of the galaxies and the instrumental resolution. In order to use model predictions based on the Lick/IDS system, the spectra were degraded to the wavelength dependent resolution of the Lick/IDS spectrograph and indices were corrected for the broadening caused by the velocity dispersion of the galaxies.



Emission Lines

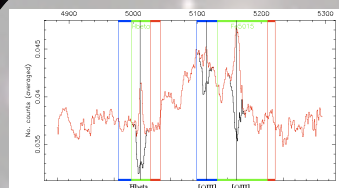


Fig. 1: Illustration of emission line correction for NGC6166. The original spectrum (red) is plotted over the emission-corrected spectrum (black) with the affected indices ($H\beta$ and $Fe5015$) and their sidebands indicated.

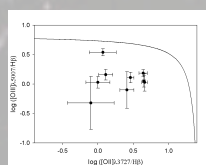


Fig. 2: Diagnostic diagram using emission lines to separate star forming galaxies from AGN. Star forming galaxies are below the line (given by Lamareille et al. 2004).

To measure the emission-line fluxes of the BCGs in this study, the GANDALF routine (Sarzi et al. 2006) was used (Figure 1). Figure 2 shows the galaxies for which the $H\beta$, $[OIII]5007$ and $[OIII]5007$ lines could be measured (within at least 2σ detections) on the diagnostic plot. All nine emission-line galaxies in the present work for which these three lines could be measured should be star forming galaxies according to this test. The GANDALF procedure was also used to derive the best-fitting emission-line spectrum in the galaxies where emission was detected, and enabled us to derive a purely-stellar spectrum for these galaxies.

References

Lamareille F., Mouchine M., Contini T., Lewis I., Maddox S., 2004, MNRAS, 350, 396
 Loubser S.I., Sansom A.E., Sánchez-Blázquez P., Soechting I.K., Bromage G.E., 2008, MNRAS, 391, 1009
 Loubser S.I., Sánchez-Blázquez P., Sansom A.E., Soechting I.K., 2009, MNRAS, in print (arXiv:0906.0287)
 Sánchez-Blázquez P., Gorgas J., Cardiel N., González J.J., 2006, A&A, 457, 787
 Sarzi M. et al., 2006, MNRAS, 366, 1151
 Thomas D., Maraston C., Bender R., 2003, MNRAS, 343, 279
 Thomas D., Maraston C., Bender R., De Oliveira C.M., 2005, ApJ, 621, 67

Indices

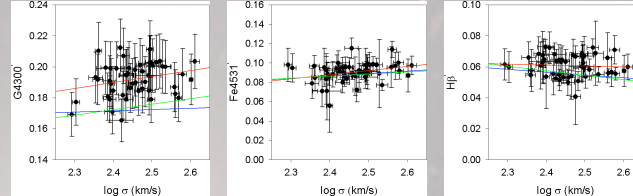


Fig. 3: Central index measurements against velocity dispersion. The straight lines fitted to the BCG data are in red. The blue lines denote the relations found for the Sánchez-Blázquez et al. (2006) elliptical sample in the same mass range, and the green line the relations for the complete Sánchez-Blázquez et al. (2006) elliptical sample (high and low density samples combined).

Straight line fits were made to the measured BCG indices against velocity dispersion with a least-squares fitting routine, and are shown in Figure 3.

With the exception of G4300, no significant differences between the index relations with velocity dispersion of the BCG data and those of normal ellipticals in the same mass range were found. The Lick offsets do not explain the difference in the G4300 index.

Simple Stellar Population Results

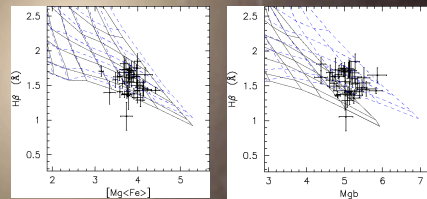
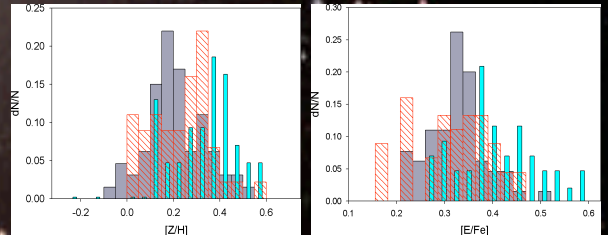


Fig. 4: Index-index plots. The grids correspond to the Thomas et al. (2003) models, with α -enhancement $[E/Fe] = 0$ (solid black) and 0.3 (dashed blue). Age lines are 15, 12, 8, 5 and 3 Gyr (from the bottom) and metallicities from $[Z/H] = 0.80$ decreasing in steps of 0.25 dex towards the left. All index measurements are in Angstrom.

To calculate the luminosity-weighted ages, metallicities ($[Z/H]$), and α -enhancement ratios ($[E/Fe]$), we compare our derived line-strength indices with the predictions of Thomas, Marston & Bender (2003, see Figure 4). Ages, $[Z/H]$ and $[E/Fe]$ were derived using the indices $\langle Fe \rangle$, $H\beta$ and Mg_b , where $\langle Fe \rangle$ is defined as $(Fe5270 + Fe5335)/2$.

Fig. 5: Distributions of the SSP-equivalent parameters of the BCGs (cyan), compared to that of ordinary ellipticals (Thomas et al. 2005 - grey; Sánchez-Blázquez et al. 2006 - red), over the same mass range. To avoid artificial offsets between samples due to the use of different techniques to calculate the SSP-parameters, we recalculated these parameters using exactly the same indices and method as used for our sample of BCGs.



Context of Environment

Hierarchical models of galaxy formation predict that the formation of the central galaxy is closely connected with the evolution of the host cluster. Thus, it is interesting to investigate whether, and to what extent, the characteristics of the host cluster play a role in the SFH of BCGs. The X-ray properties of the host clusters were collected from the literature as shown in Loubser et al. (2009).

Fig. 6: Velocity dispersion for the BCGs plotted against X-ray luminosity (i.e. density) of the host clusters. Thus, galaxies in higher density clusters are not necessarily more massive, contrary to previous findings using smaller samples.

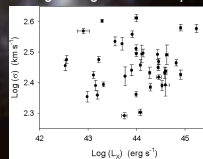
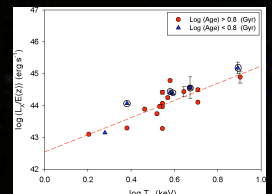


Fig. 7: Cluster L_x - T_c relation for the BCGs. The clusters hosting BCGs with ages $\log(Age) < 0.8$ Gyr are shown in blue, where the black circles denote young galaxies in cooling-flow clusters. Five of the six BCGs with younger mean ages are hosted by clusters with cooling flows and they are located in the region of the diagram where clusters with X-ray excess are found.



Conclusions

There are differences – albeit small – between the stellar populations in BCGs and ordinary elliptical galaxies over the same mass range. The BCGs show higher metallicity and α -enhancement values (Figure 5). The former possibly indicates more efficient star formation, and the latter is most commonly interpreted as a consequence of shorter formation time-scales in BCGs, though other interpretations are possible including differences in the IMF, differences in the binary fractions, or selective winds. No correlation is found between the X-ray luminosity of the clusters and the velocity dispersion of the BCGs (Figure 6). Thus, galaxies in higher density clusters are not necessarily more massive, contrary to the previous findings using smaller samples. No clear correlation between host cluster X-ray luminosity (cluster density) or host cluster velocity dispersion (cluster mass) and the derived parameters were found. Most of these massive galaxies are very old, as expected. However, 11 galaxies (26 per cent of those for which ages were derived) were found to have intermediate ages, i.e. SSP-equivalent ages of younger than 6 Gyr. These younger BCGs tend to be found in cooling-flow clusters with large X-ray excess (Figure 7). The stellar population gradients (Figure 8) and reconstructed SFHs will be investigated in future papers in the series.

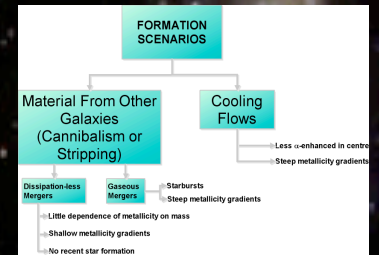


Fig. 8: Summary of observational tests for BCG formation scenarios. The gradients of SSP-parameters with radius will provide a conclusive test for the different formation scenarios (see Introduction). Even though the predicted signatures of gaseous mergers and dissipative models (such as cooling flows) are qualitatively similar in terms of metallicity gradients (in that stars in the centre are more metal rich), models predict that dissipative processes will steepen the metallicity gradient, whilst major mergers are expected to flatten it.

Acknowledgements: Observations presented here were obtained with the WHT and Gemini North and South telescopes. SIL acknowledges travel funding received from the IAU and South African SKA office.